

Critical behavior of charmonia across the phase transition: A QCD sum rule approach

Kenji Morita^{1,*} and Su Hounng Lee^{1,†}

¹*Institute of Physics and Applied Physics, Yonsei University, Seoul 120-749, Korea*

(Dated: April 21, 2019)

We investigate medium-induced change of mass and width of J/ψ and η_c across the phase transition in hot gluonic matter using QCD sum rules. In the QCD sum rule approach, the medium effect on heavy quarkonia is induced by the change of both scalar and twist-2 gluon condensates, whose temperature dependences are extracted from the lattice calculations of energy density and pressure. Although the stability of the operator product expansion side seems to break down at $T > 1.06T_c$ for the vector channel and $T > 1.04T_c$ for the pseudoscalar channel, we find a sudden change of the spectral property across the critical temperature T_c , which originates from an equally rapid change of the scalar gluon condensate characterized by $\varepsilon - 3p$. By parameterizing the ground state of the spectral density by the Breit-Wigner form, we find that for both J/ψ and η_c , the masses suddenly decrease maximally by a few hundreds of MeV and the widths broaden to ~ 100 MeV slightly above T_c . Implications for recent and future heavy ion experiments are discussed. We also carry out a similar analysis for charmonia in nuclear matter, which could serve as a testing ground for observing the precursor phenomena of the QCD phase transition. We finally discuss the possibility of observing the mass shift at nuclear matter at the FAIR project at GSI.

PACS numbers: 14.40.Gx, 11.55.Hx, 12.38.Mh, 24.85.+p

I. INTRODUCTION

In-medium change of spectral properties of heavy quarkonia is one of the interesting problems in recent hadron physics. Firstly, the recent relativistic heavy ion collision experiment at the Relativistic Heavy Ion Collider (RHIC) reveals exciting nature of the QCD matter through a number of observations [1, 2, 3, 4, 5]. However, there are many open questions in both experimental facts and theoretical understandings of QCD matter. Hence, it is important to establish appropriate experimental observables that reflect consequences of deeper theoretical understanding of the matter. Heavy quarkonia have been regarded as one of the most suitable diagnostic tools in this respect, since the suppression of J/ψ yields would reflect the Debye screening phenomenon caused by the deconfinement phenomenon in the quark-gluon plasma (QGP), as was originally argued by Matsui and Satz [6]. Until now, quarkonium production, especially that of J/ψ , in relativistic heavy ion collisions have been extensively studied both experimentally [7, 8] and theoretically [9, 10]. However, a remarkable progress comes from recent lattice QCD calculations, which indicate that contrary to the earlier expectation the J/ψ will survive as a bound state even in the QGP up to $T \sim 1.6 - 2T_c$ [11, 12, 13], which was anticipated before based on the non-perturbative nature of QGP [14]. Nowadays, the state of matter at this temperature region has been characterized as “strongly coupled” QGP (sQGP). Hence, there will be change of spectral properties even for heavy quark system which has to be considered in interpreting

experimental observables.

Secondly, charmonium in a nuclear medium is also an interesting issue. In relativistic heavy ion collisions, we need knowledge of quarkonium-nucleon interaction to discriminate the suppression by QGP from the “cold nuclear matter effect” induced by such an interaction. Furthermore, multi-gluon exchange can lead to an attractive interaction between $c\bar{c}$ and a nucleon, which may result in a bound state of charmonium and a light nuclei, as pointed out by Brodsky *et al.* [15]. It should be also noted that the Panda experiment at GSI-FAIR plans reaction of anti-protons with nucleus target, which will yield charmonia in the nuclear matter. It could serve as a testing ground for observing the precursor phenomenon of the QCD phase transition.

In this paper, we investigate change of mass and width of J/ψ and η_c induced by strongly interacting hot gluonic matter and by nuclear medium using QCD sum rule. QCD sum rule provides a systematic procedure for studying hadrons from a viewpoint of the asymptotic freedom in QCD [16, 17]. Since the QCD sum rule can take non-perturbative effects into account through the condensate terms, it is a suitable theoretical tool of the current study. Indeed, QGP at $T < 3T_c$ cannot be understood using perturbation theory alone [18]. Furthermore, the sum rule is more promising for heavy quark systems because we do not have to take the quark-antiquark condensate into account unlike light quark systems. In this respect, the sum rule has been applied to charmonium and bottomonium. Shifman *et al.* established the framework in Ref. [16, 17] and Reinders *et al.* extended it to deep Euclidean region $Q^2 = -q^2 > 0$ [19], in the case of vacuum. As for the quarkonia in-medium, One of us together with Furnstahl and Hatsuda have investigated the mass shift of J/ψ in hot hadronic matter [20], using a QCD sum rule approach, where the temperature effect was intro-

*Electronic address: morita@phya.yonsei.ac.kr

†Electronic address: suhounng@phya.yonsei.ac.kr

duced to the perturbative Wilson coefficient through the scattering terms. A consistent formalism at lower density was developed by one of us [21] and independently by Hayashigaki [22] to study the mass shift of J/ψ in nuclear matter.

Along this direction, we investigated the mass shift and width broadening of J/ψ in hot gluonic plasma (GP) [23] just above the phase transition by consistently using the exact temperature dependencies of condensates from lattice calculation. In the present paper, as a subsequent paper to Ref. [23], we present details of the analysis, further application to η_c and to spectral changes in nuclear matter.

In the next section, we will give an explanation of the QCD sum rule for heavy quarkonium in medium used in the present work. Section III and IV describe the details of the numerical computations of the sum rule for hot gluonic matter and nuclear medium, respectively. Section V is devoted to discussion and summary.

II. QCD SUM RULE FOR HEAVY QUARKONIUM

In this section, first we review the sum rule for heavy quarkonium in vacuum [19]. Then we introduce the extension to finite temperature and nuclear medium cases, in which medium effect is eventually induced only by the expectation values of gluonic operators without any additional change in the operator product expansion (OPE).

A. Moment sum rule in vacuum

We start with the time-ordered current-current correlation function for J channel

$$\Pi^J(q) = i \int d^4x e^{iq \cdot x} \langle T[j^J(x)j^J(0)] \rangle, \quad (1)$$

where we consider $J = P$ (pseudoscalar) and V (vector) current of the heavy quark. Namely, $j^P = i\bar{c}\gamma_5 c$ and $j^V_\mu = \bar{c}\gamma_\mu c$, for charm. The expectation value $\langle \dots \rangle$ is taken for the vacuum. If we go to deep Euclidean region $Q^2 \equiv -q^2 \gg 0$, the product of the current can be expanded via operator production expansion (OPE) [24]. If we denote $\tilde{\Pi}^J(q^2)$ such that $\Pi^{\mu\nu}(q) = (q^\mu q^\nu - q^2 g^{\mu\nu})\tilde{\Pi}^J(q^2)$ for the vector current, $\tilde{\Pi}^J(q^2)$ can be written as

$$\tilde{\Pi}^J(q^2) = \sum_n C_n^J \langle O_n \rangle \quad (2)$$

where O_n are the operators of mass dimension n renormalized at scale μ^2 and C_n^J are the Wilson coefficient. By virtue of much heavier quark mass than the confinement scale, heavy quark operators, such as $m_c \bar{c}c$ for dimension 4, are rewritten in terms of gluonic operator with a factor of $1/m_c$ via heavy quark expansion [16, 25]. Hence, only

gluonic operators contribute to the OPE for the heavy quark currents.

On the other hand, the correlation function (2) is related to its imaginary part through the dispersion relation

$$\tilde{\Pi}^J(q^2) = \frac{1}{\pi} \int_{4m_c^2}^{\infty} \frac{\text{Im}\tilde{\Pi}^J(s)}{s - q^2} ds \quad (3)$$

where we ignore $+i\varepsilon$ in the denominator of the integrand since $q^2 = -Q^2 < 0$. Taking n times derivative of Eqs. (2) and (3) as

$$M_n^J(Q^2) \equiv \frac{1}{n!} \left(\frac{d}{dq^2} \right)^n \tilde{\Pi}^J(q^2) \Big|_{q^2 = -Q^2}, \quad (4)$$

we obtain the n -th order moment for the OPE side

$$M_n^J(Q^2)_{\text{OPE}} = A_n^J(\xi)[1 + a_n^J(\xi)\alpha_s + b_n^J(\xi)\phi_b], \quad (5)$$

and that for the phenomenological (dispersion) side

$$M_n^J(Q^2)_{\text{phen.}} = \frac{1}{\pi} \int_{4m_c^2}^{\infty} \frac{\text{Im}\tilde{\Pi}^J(s)}{(s + Q^2)^{n+1}} ds. \quad (6)$$

Here, we have introduced a dimensionless scale variable $\xi = Q^2/4m_c^2$. In Eq. (5), $A_n^J(\xi)$, $a_n^J(\xi)$, and $b_n^J(\xi)$ are the Wilson coefficients which correspond to bare loop diagrams, perturbative radiative correction up to order α_s , and scalar gluon condensate, respectively. These coefficients were derived in Ref. [19] and we summarize them in the Appendix.

In evaluation of spectral properties, we take the ratio of the $(n-1)$ -th moment to the n -th moment and equate the OPE side with the phenomenological side. Then we obtain the sum rule

$$\frac{M_{n-1}^J}{M_n^J} \Big|_{\text{OPE}} = \frac{M_{n-1}^J}{M_n^J} \Big|_{\text{phen.}}, \quad (7)$$

which relates the hadron properties (r.h.s.) with asymptotically free QCD (l.h.s.)

B. Moment sum rule for the hot gluonic medium

In this paper, we firstly consider the gluonic medium at finite temperature around T_c . Then, the expectation value in Eq. (1) is taken as $\langle O \rangle = \text{Tr}(e^{-\beta H} O) / \text{Tr}(e^{-\beta H})$. Hereafter, we set both medium and $\bar{c}c$ at rest. We denote $q^\mu = (\omega, \mathbf{q})$ and take $\mathbf{q} \rightarrow 0$ limit. In this case, the transverse and the longitudinal components of the correlation function for the vector channel are simply related with $\Pi_T = \omega^2 \Pi_L$ and $\Pi_L = \Pi_\mu^\mu / (-3\omega^2)$. We denote the longitudinal component as $\tilde{\Pi}^J(\omega)$ for the vector channel.

At finite temperature, *retarded* correlation function is related to the spectral function [26]. In the Euclidean region $\omega^2 < 0$, the retarded correlation function $\Pi^R(\omega)$

becomes $\Pi(\omega^2)$ and the dispersion relation is given by [20, 27]

$$\tilde{\Pi}^J(\omega^2) = \int_{0^-}^{\infty} du^2 \frac{\rho(u)}{u^2 - \omega^2}, \quad (8)$$

where $\rho(u)$ is the spectral function connecting with the imaginary part as

$$\rho(u) = \frac{1}{\pi} \tanh\left(\frac{u}{2T}\right) \text{Im}\tilde{\Pi}^J(u^2). \quad (9)$$

Then Eq. (8) reduces to the vacuum case [Eq. (3)] when $\text{Im}\tilde{\Pi}^J(u^2)$ has nonzero value only at $u \gg T$. Since we are interested in charmonia for which the mass is much larger than temperature considered here, this condition seems to be appropriate one. However, there are formally two additional terms in the finite temperature spectral function [28]. One is the continuum part which also exists in the case of vacuum. Following the prescription in Ref. [19], we can suppress contribution from this part as described later because this part has finite values beyond some threshold. The other part arising from scattering of the current with quarks in medium is proportional to $\delta(u^2)$ and the contribution grows up with T in the hadronic medium [20]. However, since we are considering the *gluonic* medium in which there are no (anti-)quarks which annihilate with the current, such a scattering term does not appear. Hence, we can use the same expression of the phenomenological side with the vacuum case [Eq. (6)] for charmonia in the hot gluonic medium.

As for the OPE side, there is an important change from the vacuum to the medium case. Since we have no longer Lorentz invariance, non-scalar operators have non-vanishing value [27]. In the present case, twist-2 gluon operator has leading contribution and the n -th order moment of the OPE side [Eq. (5)] should be modified to

$$M_n^J(Q^2)_{\text{OPE}} = A_n^J(\xi)[1 + a_n^J(\xi)\alpha_s + b_n^J(\xi)\phi_b + c_n^J(\xi)\phi_c], \quad (10)$$

where c_n and ϕ_c are the Wilson coefficients and the medium expectation value for the twist-2 operator. Since we are considering the heavy quark systems, only the condensate terms are temperature dependent as long as $T \ll m_c, |Q|$ [20, 27]. Hence, the Wilson coefficients are the same as in the vacuum case. In the following, we show that the gluon condensates $\phi_{b,c}$ are written in terms of thermodynamic quantities which can be extracted from lattice QCD data.

If we define these condensate terms as

$$G_0(T) = \left\langle \frac{\alpha_s}{\pi} G_{\mu\nu}^a G^{a\mu\nu} \right\rangle_T, \quad (11)$$

$$\left(u^\mu u^\nu - \frac{1}{4} g^{\mu\nu} \right) G_2(T) = \left\langle \frac{\alpha_s}{\pi} G_\rho^{a\mu} G^{a\nu\rho} \right\rangle_T, \quad (12)$$

where u^μ is the 4-velocity of the medium and taken to

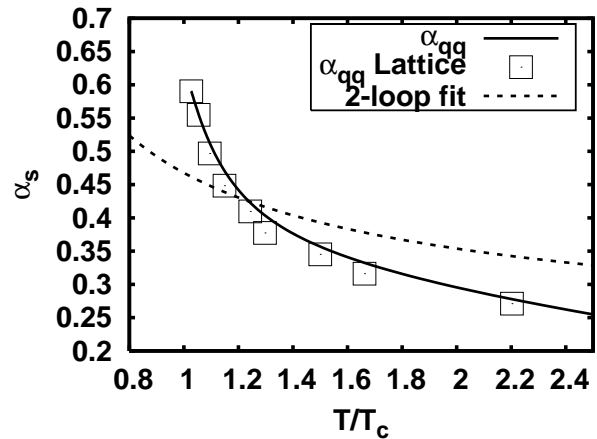


FIG. 1: Temperature dependent coupling constants extracted from lattice QCD. The boxes denote the lattice data points of $\alpha_{\text{qq}}(r_{\text{screen}}, T)$ taken from Ref. [29]. The solid line is drawn by Bezier interpolation of the lattice data points. The dotted line shows the case of Eq. (20).

be $u^\mu = (1, 0, 0, 0)$, explicit forms of $\phi_{b,c}$ are given as

$$\phi_b = \frac{4\pi^2}{9(4m_c^2)^2} G_0(T), \quad (13)$$

$$\phi_c = \frac{4\pi^2}{3(4m_c^2)^2} G_2(T). \quad (14)$$

Actually it is possible to calculate the condensates (11) and (12) directly using lattice QCD, but we do not adopt such an approach here. The gluon condensates generally consist of the perturbative piece and the non-perturbative piece. At zero temperature, the condensate term appearing in QCD sum rules is the non-perturbative piece only and it is shown that the non-perturbative part extracted from lattice QCD by subtracting the perturbative part is indeed consistent with the value of the condensate determined from QCD sum rules for charmonium [30, 31, 32]. Similar consideration holds also for the finite temperature case [33], in which we would have to subtract out the perturbative part at $T \neq 0$ if we directly calculated the non-perturbative condensates from lattice QCD. In this paper, since we are putting all the temperature dependencies in the condensates, including the perturbative and non-perturbative contributions, we can just extract total temperature dependencies of the operators from the lattice. This is possible by noting that the scalar gluon condensate and twist-2 gluon condensates are respectively just the trace part and symmetric traceless part of the energy momentum tensor. This energy momentum tensor is well calculated on the lattice from the pressure and energy density of the plasma through the following equation,

$$T^{\alpha\beta} = (\varepsilon + p) \left(u^\alpha u^\beta - \frac{1}{4} g^{\alpha\beta} \right) + \frac{1}{4} (\varepsilon - 3p) g^{\alpha\beta}. \quad (15)$$

The scalar condensate can be related to the trace part

through the trace anomaly as

$$T_\mu^\mu = \frac{\beta(g)}{2g} \langle G_{\mu\nu}^a G^{a\mu\nu} \rangle, \quad (16)$$

with $\beta(g)$ being the beta function. Using the one-loop expression with $N_f = 0$ and $N_c = 3$ for the beta function and recalling that $T_\mu^\mu = \varepsilon - 3p$, we obtain

$$G_0(T) = G_0^{\text{vac}} - \frac{8}{11}(\varepsilon - 3p) \quad (17)$$

where G_0^{vac} is the value of the scalar gluon condensate in vacuum [34]. As for the twist-2 part, the symmetric traceless part of the energy-momentum tensor is the gluon operator

$$T^{\alpha\beta} = -G^{a\alpha\lambda} G_\lambda^{a\beta}. \quad (18)$$

If we assume the medium is the perfect fluid, as strongly supported by the experiments for temperature not so higher than T_c , we can identify the traceless part of the energy momentum tensor to $(\varepsilon + p)$ as given in Eq.(15). Hence, by comparing this with Eq. (12), the twist-2 part becomes

$$G_2(T) = -\frac{\alpha_s(T)}{\pi}(\varepsilon + p). \quad (19)$$

We extract the temperature dependent quantities ε , p [35] and $\alpha_s(T)$ [29] from lattice calculations for the pure SU(3) system. In order to construct G_2 , we need the temperature dependent effective coupling constant. The coupling constant, however, cannot be uniquely determined by lattice QCD [29]. Ref. [29] presented four kinds of the coupling constant extracted from the color singlet heavy quark-antiquark free energy. Two of them are measured in the short distant regime and the others are done in the long distant regime. In the former, one is from the free energy and the other is from the spatial derivative of the free energy (force). Both coupling constants are almost independent of temperature at short distance, $r < 0.1$ fm. While the former goes to negative value at larger distance due to the remnant of the confinement force, the latter shows temperature dependent maximum value, at which the distance is denoted by r_{screen} . Here, we adopt the latter one, $\alpha_{\text{qg}}(r, T)$ at $r = r_{\text{screen}}$ as one of reasonable coupling constants. On the other hand, the long distant regime is based on a fit of the free energy to the Debye-screened functional form which has two coupling parameters, Coulomb force strength $\alpha(T)$ and screening $\tilde{\alpha}(T)$. Although both of the coupling constants show reasonable temperature dependencies and agree each other at $T > 6T_c$, we adopt $\tilde{\alpha}(T)$ because the value of Coulomb part strength seems to be too large, $\alpha(T_c) \sim 1.5$. Unlike α_{qg} , the uncertainty in the result of $\tilde{\alpha}(T)$ is too large. Therefore, we use the 2-loop perturbative running coupling form

$$g_{\text{pert}}^{-2}(T) = \frac{11}{8\pi^2} \ln\left(\frac{2\pi T}{\Lambda_{\overline{\text{MS}}}}\right) + \frac{51}{88\pi^2} \ln\left[2 \ln\left(\frac{2\pi T}{\Lambda_{\overline{\text{MS}}}}\right)\right], \quad (20)$$

with $T_c/\Lambda_{\overline{\text{MS}}} \simeq 1.14$ and rescale this as $\tilde{\alpha}(T) = 2.095\alpha_{\text{pert}}(T)$ [29]. Here we put $T_c = 264$ MeV [35]. The two coupling constants as a function of temperature are displayed in Fig. 1. As explained later, we will consider only temperature region near T_c in this paper. Hence, α_{qg} is stronger than $\tilde{\alpha}(T)$ throughout analyses in this paper.

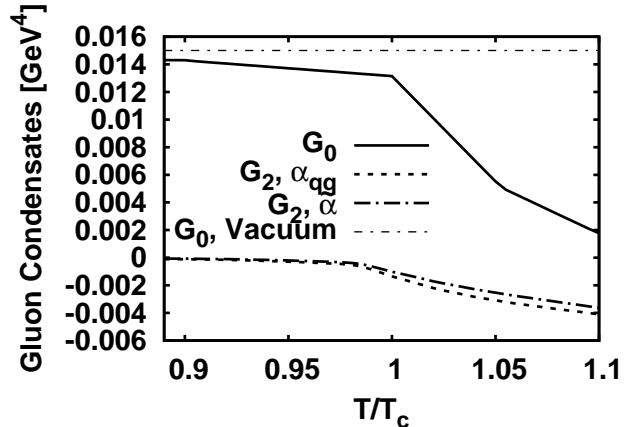


FIG. 2: Gluon condensates near T_c .

The resultant gluon condensates G_0 and G_2 for two cases of the coupling constant are shown in Fig. 2. For G_0 , we use $G_0^{\text{vac}} = (0.35\text{GeV})^4 \simeq 0.015\text{GeV}^4$. We can see that G_0 decreases as temperature increases and reaches less than half of the vacuum value at $T/T_c \simeq 1.04$. It becomes negative at higher temperature but remains positive in the temperature region considered here [33].

C. Moment sum rule for the nuclear medium

In this case, the medium consist of nucleons, thus we do not have to worry about the scattering term. As far as we follow the same method to suppress the contribution from the continuum, we can use the same form of the phenomenological side with the vacuum and finite temperature cases.

Thus, since the medium effect is similarly imposed on the gluon condensates, difference in the nuclear matter case from the case of hot gluonic matter is in the explicit form of $\phi_{\text{b,c}}$. In order to evaluate the expectation value for the ground state of the nuclear matter, we employ the linear density approximation [36]:

$$\langle O \rangle_{\text{n.m.}} = \langle O \rangle_0 + \frac{\rho_N}{2m_N} \langle N | O | N \rangle, \quad (21)$$

where ρ_N and m_N are the normal nuclear matter density and the nucleon mass, respectively. The nucleon state $|N\rangle$ is normalized as $\langle N(p') | N(p) \rangle = 2p_0 (2\pi)^3 \delta^3(p - p')$. Then, the scalar condensate becomes [21]

$$\left\langle \frac{\alpha_s}{\pi} G_{\mu\nu}^a G^{a\mu\nu} \right\rangle_{\text{n.m.}} = \left\langle \frac{\alpha_s}{\pi} G_{\mu\nu}^a G^{a\mu\nu} \right\rangle_0 - \frac{8}{9} m_N^0 \rho_N \quad (22)$$

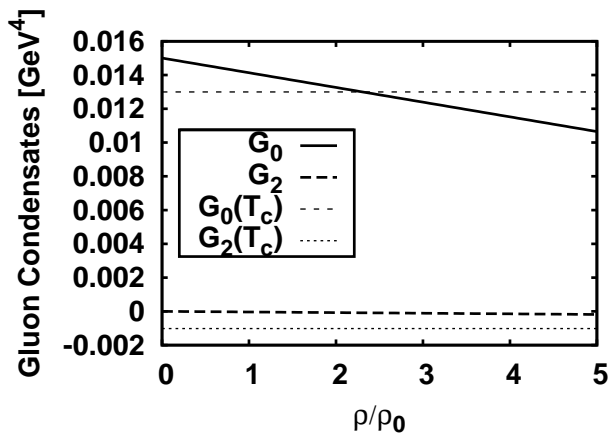


FIG. 3: Gluon condensates in nuclear matter. Thick solid and dashed line show the scalar and twist-2 condensates as a function of density normalized by the normal nuclear density. Thin lines are the finite temperature case at $T = T_c$ for a comparison.

where $m_N^0 \simeq 750$ MeV is the nucleon mass in the chiral limit [37]. The traceless and symmetric twist-2 operator is given as [21],

$$\left\langle N(p) \left| \frac{\alpha_s}{\pi} G_{\alpha\sigma}^a G^{a\beta\sigma} \right| N(p) \right\rangle = - \left(p_\alpha p^\beta - \frac{1}{4} g_\alpha^\beta p^2 \right) \frac{\alpha_s}{\pi} A_G \quad (23)$$

where A_G is related to the moment of the gluon distribution function

$$A_G(\mu^2) = 2 \int_0^1 dx x G(x, \mu^2). \quad (24)$$

Following Ref. [21], we take $A_G(8m_c^2) \simeq 0.9$. Using these expressions, the condensate terms which appears in Eq. (5) finally result in [21]

$$\phi_b = \frac{4\pi^2}{9(4m_c^2)^2} \left\langle \frac{\alpha_s}{\pi} G_{\mu\nu}^a G^{a\mu\nu} \right\rangle_{\text{n.m.}} \quad (25)$$

$$\phi_c = - \frac{2\pi^2}{3} \frac{\alpha_s}{(4m_c^2)^2} A_G m_N \rho_N. \quad (26)$$

The form of ϕ_b is the same as the hot gluonic matter case but now the expectation value is taken through Eq. (22). We depict the density dependence of the gluon condensates based on Eqs. (22) and (26) in Fig. 3. The twist-2 case is re-normalized so that it corresponds to the finite temperature case (14). We can see that the change of the scalar condensate reaches as large as $T = T_c$ case at $\rho \sim 2\rho_0$ but is much smaller at the normal nuclear density. The twist-2 contribution is much smaller than that of the finite temperature case.

D. Phenomenological side

In the phenomenological side, we use a simple prescription which describes the lowest lying resonance

in each channel. For charmonium, previous studies [16, 19, 20, 21, 22] focused on the mass and ignored the small but finite width of J/ψ and η_c . In this case, the imaginary part of the polarization function in Eq. (6) is simply parametrized by

$$\text{Im}\tilde{\Pi}(s) = f_0 \delta(s - m^2) + \text{corrections}, \quad (27)$$

where we ignore the channel subscript J . This spectral function immediately leads to the moment

$$M_n(\xi) = \frac{f_0}{\pi(m^2 + Q^2)^{n+1}} [1 + \delta_n(\xi)]. \quad (28)$$

The correction term in Eq. (27) is absorbed in $\delta_n(\xi)$. By taking the ratio as in Eq. (7), we can remove the constant f_0 from the equation. To obtain the mass of lowest lying resonance, we need to choose sufficiently large n such that $(1 + \delta_{n-1}(\xi))/(1 + \delta_n(\xi))$ is close to unity. Then the ratio does not depend on the details of the correction term which contains higher resonances and continuum, and the mass is simply given by

$$m^2 \simeq \frac{M_{n-1}(\xi)}{M_n(\xi)} - 4m_c^2 \xi. \quad (29)$$

Previous analyses rely on this formula.

In this work, we extend the above formulation to include finite width. Here, we employ the simple relativistic Breit-Wigner form

$$\text{Im}\tilde{\Pi}(s) = \frac{f_0 \sqrt{s} \Gamma}{(s - m^2)^2 + s \Gamma^2} + \text{corrections}. \quad (30)$$

As in the $\Gamma = 0$ case, we can eliminate the unnecessary constant and the effects of the correction term by taking the ratio of the moment and choosing appropriately large n . In the practical analyses of the sum rule, our task is to find values of (m, Γ) which satisfy the sum rule [Eq. (7)]. Generally there are infinite numbers of the pairs of (m, Γ) because the sum rule provides one equation with respect to the two quantities which we want to know. Hence, without additional constraints, the sum rule can provide only relation between m and Γ as in the case of light vector mesons [38]. Here, before the practical calculation, we discuss the relation between the mass and the width which comes from the phenomenological side, Eq. (30).

In calculation of the moment ratio of the phenomenological side, we need to compute the dispersion integral in Eq. (6) with the spectral function in Eq. (30). Since the width of the ground state charmonium is much smaller than its mass, we need careful treatment in numerical integration. To achieve good accuracy, we performed Monte-Carlo integration based on the VEGAS algorithm [39]. In our calculation, typical relative numerical uncertainty evaluated from the standard manner in the Monte-Carlo integration is order of 10^{-6} for 10^6 events with $m = 3$ GeV and $\Gamma = 1$ MeV. As expected, this accuracy becomes better as Γ increases.

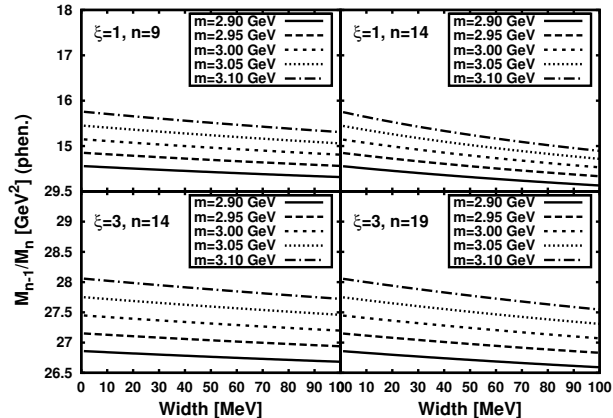


FIG. 4: Moment ratio of the phenomenological side as a function of Γ . Upper panels are for $\xi = 1$. Left and right panels denote the case of $n = 9$ and $n = 14$, respectively. Lower ones are for $\xi = 3$ with $n = 14$ (left) and $n = 19$ (right).

We plot the Γ dependence of the moment ratio for various mass values from 2.9 GeV to 3.1 GeV in Fig. 4. Here we show the result for two values of ξ , $\xi = 1$ and 3. In each ξ value, we choose two values of n , of which are the typical values for the analyses below, to see n dependence of the moment ratio. First, comparing the left (smaller n) side to the right (large n) side, we can see that Γ dependence of the moment ratio becomes stronger as n increases. As we will see later, larger n is suitable for evaluating mass at higher temperature. Hence, this fact means that, as the temperature increase, the system becomes more sensitive to the width. Second, the moment ratio decreases monotonically as the width increases if mass is unchanged. It also decreases as the mass decreases but the width dependence is much weaker. For instance, let us suppose that we obtain 1 GeV² decrease of the moment ratio from the OPE side for $\xi = 1$. If mass stays constant, the width must broaden to larger than 100 MeV while it corresponds to about 100 MeV mass reduction in the case that the width remains in its vacuum value. Finally, as is shown in comparison of the upper-right with the lower-left, the width dependence becomes weaker if we choose larger ξ . Its consequence will be discussed in the next section.

III. CHARMONIUM IN HOT GLUONIC MATTER

In this section, we present the result of the analysis for the hot gluonic matter. The parameters of the theory are α_s and m_c . Hereafter, they are set to 0.21 and 1.24 GeV at $\xi = 1$, that are taken from [21], respectively.

We begin with fixing n such that the moment ratio of the OPE side takes its minimum value for each temperature. As briefly mentioned before, we need to choose moderately large n so that contribution from ex-

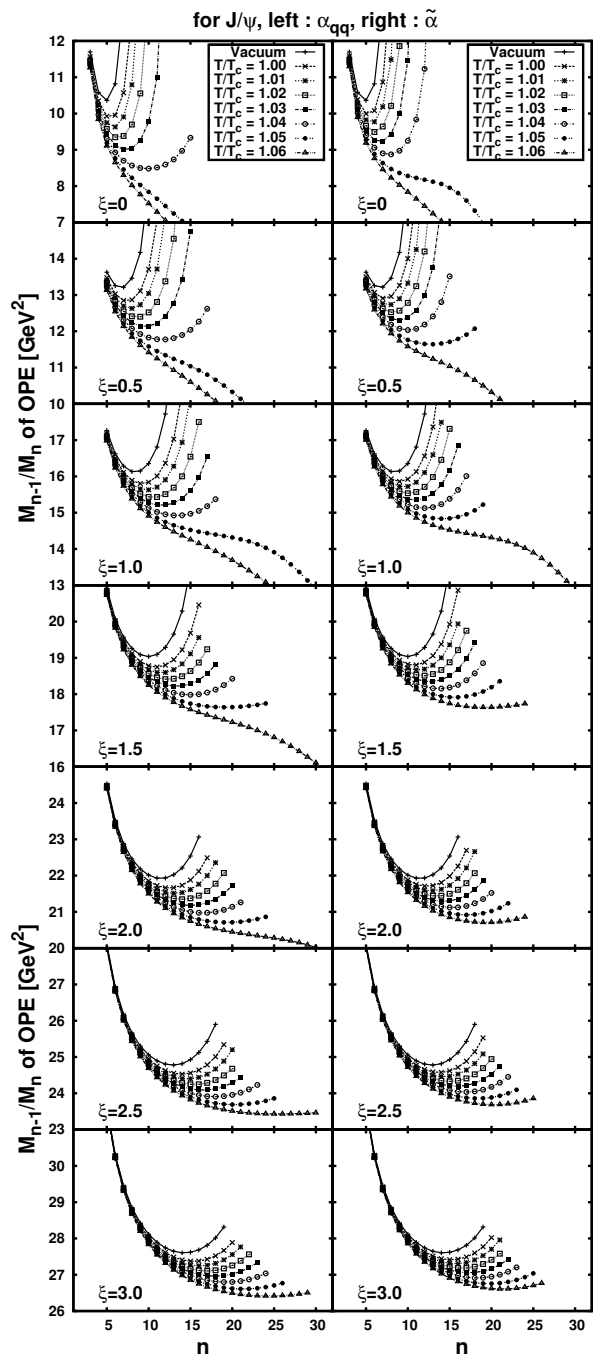


FIG. 5: Moment ratio for the OPE side for the vector channel (J/ψ). Each panels show different ξ and coupling constant case. The symbols stand for different temperature.

cited states and continuum can be sufficiently suppressed. Therefore, this ratio should approach a constant value at adequately large n . However, in the OPE side contribution from higher dimensional operators will be important at large n . As such n value that the moment ratio takes its minimum value, pole dominance and truncation of the OPE are valid and the ratio is close to the real asymptotic value, as have been extensively studied in the vacuum

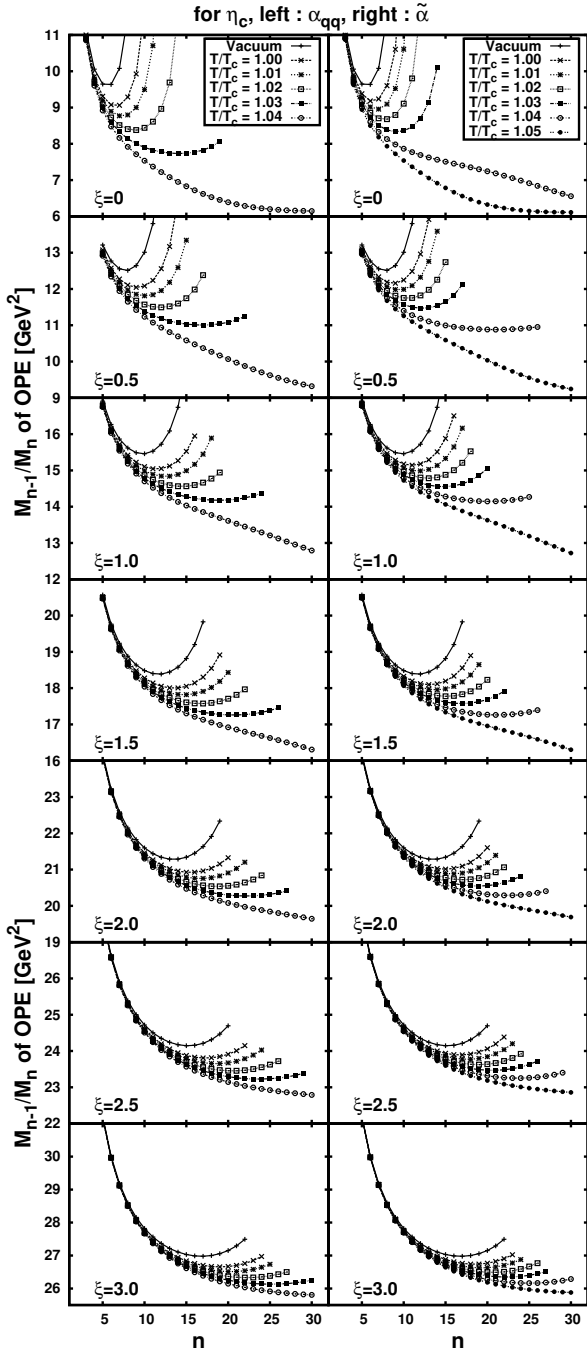


FIG. 6: Same as Fig. 5, but for the pseudoscalar channel (η_c).

case [19].

We display the moment ratio for the OPE side [Eq. (10)] in Figs. 5 and 6 with the gluon condensates shown in Fig. 2.

Figure 5 shows the moment ratio for the vector channel. The left and right column show the case in which we use α_{qq} and $\tilde{\alpha}$, respectively. Comparing different ξ cases, we can see that the stability of the moment becomes better as ξ increases. But the values of n which give the stability to the moment ratio also becomes larger. As

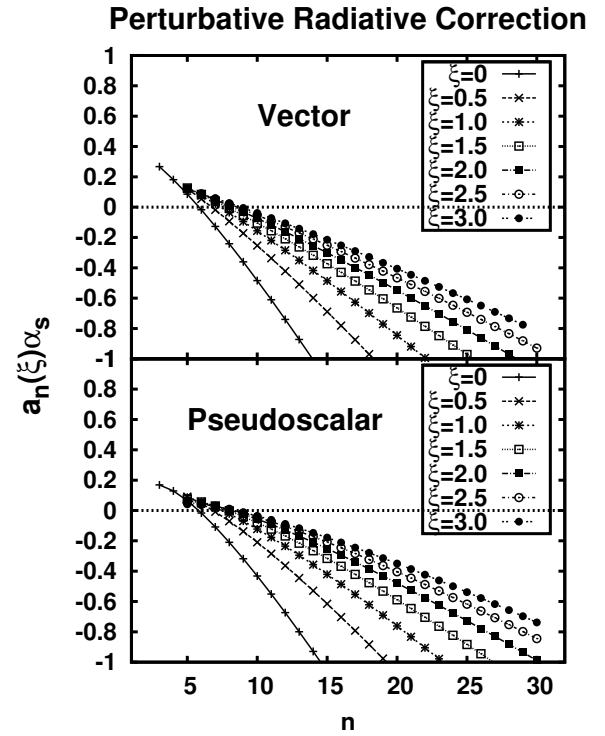


FIG. 7: Radiative correction term $a_n(\xi)\alpha_s$ in the OPE. Upper panel shows the vector case and lower one shows the pseudoscalar case.

previously reported in [23], the stability is only achieved near T_c and the stronger coupling, which is α_{qq} in this temperature region, gives worse stability. By increasing ξ , we can improve the stability a little. While it is achieved only up to $1.04T_c$ for $\xi = 0$, the moment ratio remains stable up to $1.06T_c$ for $\xi = 3$.

We can see the similar situation in the pseudoscalar channel depicted in Fig. 6. However, the moment ratio is less stable than the vector case. In the pseudoscalar case, even the best case (using $\tilde{\alpha}$ and $\xi = 3$) can stabilize the moment ratio only up to $1.04T_c$.

Note that the lack of stability does not necessarily mean dissociation of the charmonia. The reason of such instability can be clearly seen in the each terms of the OPE [Eq. (10)], of which each term must be much less than unity for convergence. These terms are displayed in Figs. 7-9. We can see that all the coefficients grow up with n . An important feature in all the coefficients is that increasing ξ clearly keeps their value smaller. Among these three, only $c_n(\xi)\phi_c$ always has positive sign and its magnitude increases with temperature. These two features are opposite to $b_n(\xi)\phi_b$, in which the sign is always negative and the value seems to approach to zero as temperature increases. In comparing the two channels, one finds that there are no significant differences. Hence, the stability will be determined by a delicate balance between coefficients and its breakdown will be caused by rapid increase of $c_n(\xi)\phi_c$.

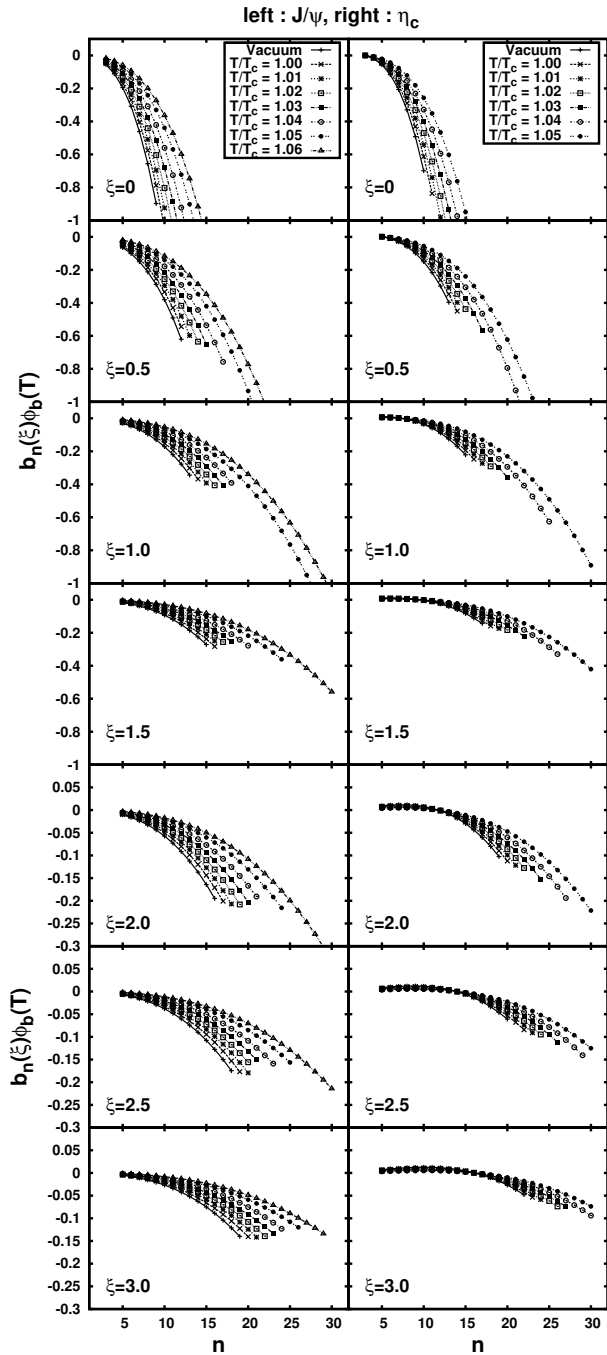


FIG. 8: Scalar condensate term $b_n(\xi)\phi_b$. Left and right column stand for the vector and the pseudoscalar case, respectively. Symbols denote different temperature cases.

Now we proceed to the determination of mass and width. The values of n are listed in Table I. Note that the stability achieved at the highest temperature is ambiguous in some cases; for example, η_c of $\xi = 0.5$ with $\tilde{\alpha}$ case is stable at $T/T_c = 1.04$ with $n = 21$. However, as seen in Fig. 6, the moment ratio is almost constant in such large n region and never rises up as lower temperature cases do. Such a vague stability is also seen in

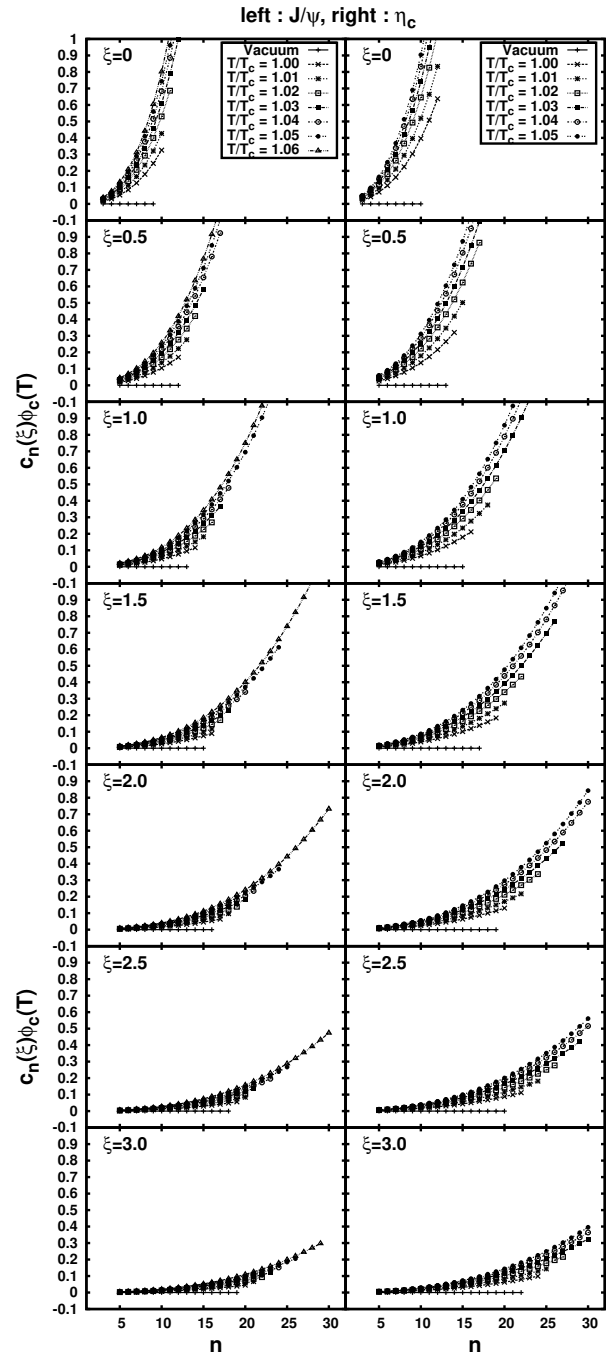


FIG. 9: Twist-2 condensate term $c_n(\xi)\phi_c$ with α_{qq} .

other cases. Hence, we note that mass and width values evaluated on the basis of such a stability are less reliable in the analyses below.

Once n and ξ are fixed, we can compute the mass and the width by making use of Eq. (7). For a fixed moment ratio of the OPE side, we firstly compute the mass in the limit of $\Gamma \rightarrow 0$ using Eq. (29). By virtue of the monotonic behavior of the moment ratio of the phenomenological side shown in Fig. 4, we can safely calculate the mass in the case of finite width by numerically solving Eq. (7)

TABLE I: List of n values at which the moment ratio takes minimum values.

| J | $\alpha_s(T)$ | ξ | Vac. | $\frac{T}{T_c}=1$ | 1.01 | 1.02 | 1.03 | 1.04 | 1.05 | 1.06 |
|----------|------------------|-------|------|-------------------|------|------|------|------|------|------|
| J/ψ | α_{qq} | 0 | 5 | 5 | 6 | 6 | 7 | 10 | 26 | N/A |
| | | 0.5 | 7 | 7 | 8 | 9 | 10 | 12 | N/A | N/A |
| | | 1 | 8 | 9 | 10 | 11 | 12 | 13 | N/A | N/A |
| | | 1.5 | 10 | 11 | 11 | 12 | 13 | 15 | 19 | N/A |
| | | 2 | 11 | 12 | 13 | 14 | 15 | 16 | 19 | N/A |
| | | 2.5 | 13 | 14 | 15 | 15 | 16 | 18 | 20 | 25 |
| | 3 | 14 | 15 | 16 | 17 | 18 | 19 | 21 | 24 | |
| | $\tilde{\alpha}$ | 0 | 5 | 5 | 6 | 6 | 7 | 8 | 27 | 26 |
| | | 0.5 | 7 | 7 | 8 | 8 | 9 | 10 | 13 | N/A |
| | | 1 | 8 | 9 | 9 | 10 | 11 | 12 | 14 | N/A |
| | | 1.5 | 10 | 11 | 11 | 12 | 13 | 14 | 16 | 19 |
| | | 2 | 11 | 12 | 13 | 13 | 14 | 15 | 17 | 19 |
| 2.5 | | 13 | 14 | 14 | 15 | 16 | 17 | 18 | 20 | |
| 3 | 14 | 15 | 16 | 16 | 17 | 18 | 20 | 21 | | |
| η_c | α_{qq} | 0 | 6 | 7 | 7 | 9 | 14 | N/A | 27 | 25 |
| | | 0.5 | 8 | 9 | 10 | 12 | 17 | N/A | N/A | N/A |
| | | 1 | 10 | 11 | 13 | 14 | 19 | N/A | N/A | N/A |
| | | 1.5 | 12 | 14 | 15 | 17 | 21 | N/A | N/A | N/A |
| | | 2 | 14 | 15 | 17 | 19 | 22 | N/A | N/A | N/A |
| | | 2.5 | 15 | 17 | 19 | 21 | 24 | N/A | N/A | N/A |
| | 3 | 17 | 19 | 20 | 22 | 25 | N/A | N/A | N/A | |
| | $\tilde{\alpha}$ | 0 | 6 | 6 | 7 | 8 | 9 | N/A | N/A | 27 |
| | | 0.5 | 8 | 9 | 9 | 10 | 12 | 21 | N/A | N/A |
| | | 1 | 10 | 11 | 12 | 13 | 15 | 20 | N/A | N/A |
| | | 1.5 | 12 | 13 | 14 | 15 | 17 | 21 | N/A | N/A |
| | | 2 | 14 | 15 | 16 | 17 | 19 | 22 | N/A | N/A |
| 2.5 | | 15 | 17 | 18 | 19 | 21 | 24 | N/A | N/A | |
| 3 | 17 | 18 | 19 | 21 | 22 | 25 | N/A | N/A | | |

with Eq. (30).

We plot the relation between the mass shift and the width at various temperatures in Figs. 10 and 11. We can see the almost linear behavior of the width as a function of the mass shift. Note that the vacuum mass differs for different ξ . We do not perform fine tuning of the parameters so that the real vacuum mass is reproduced. Although there are some exceptions for the linear relation, especially small ξ and high temperature cases, these come from the vague stability we mentioned before. Hence, we can conclude that the mass shift and the width have the linear relationship. The other important aspect is temperature dependence of the mass shift and the width. We cannot know how the mass and the width behave in the real situation, since we cannot simultaneously determine both of the mass and the width. Here, we investigate two extreme cases; $\Gamma \rightarrow 0$ limit and $\delta m \rightarrow 0$ limit.

The results are shown in Figs. 12 and 13. In these figures, we plot the results of $T > 0.9T_c$. Figure 12 shows the remarkable behavior of the mass shift; The

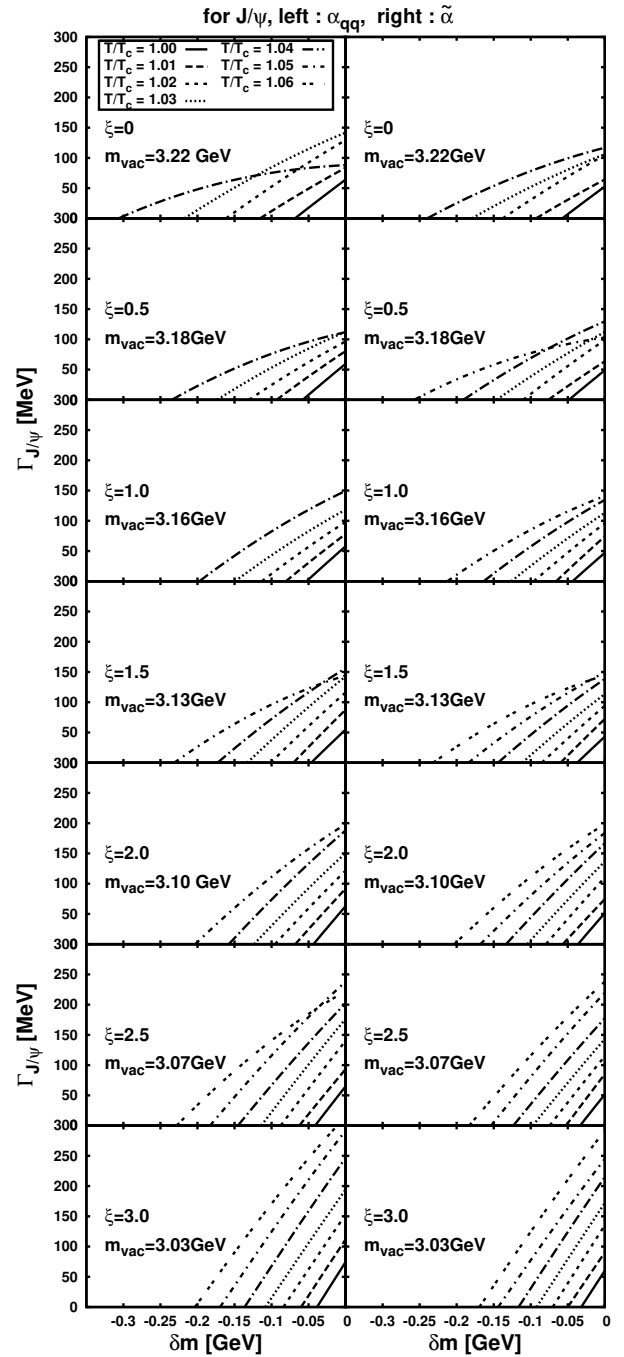


FIG. 10: Relation between mass shift $\delta m = m_{\text{vacuum}} - m$ and width Γ for J/ψ . As in Figs. 5 and 6, each figure shows different ξ case for two cases of the coupling constant, α_{qq} and $\tilde{\alpha}$.

mass does not change up to $T \sim T_c$ but it suddenly begins to decrease across T_c . This fact clearly reflects the temperature dependence of the gluon condensates which represent the phase transition. Above T_c , the mass decreases with temperature almost linearly. This feature is common for both J/ψ and η_c . Though small ξ results, especially $\xi = 0$, show more rapid decrease, the

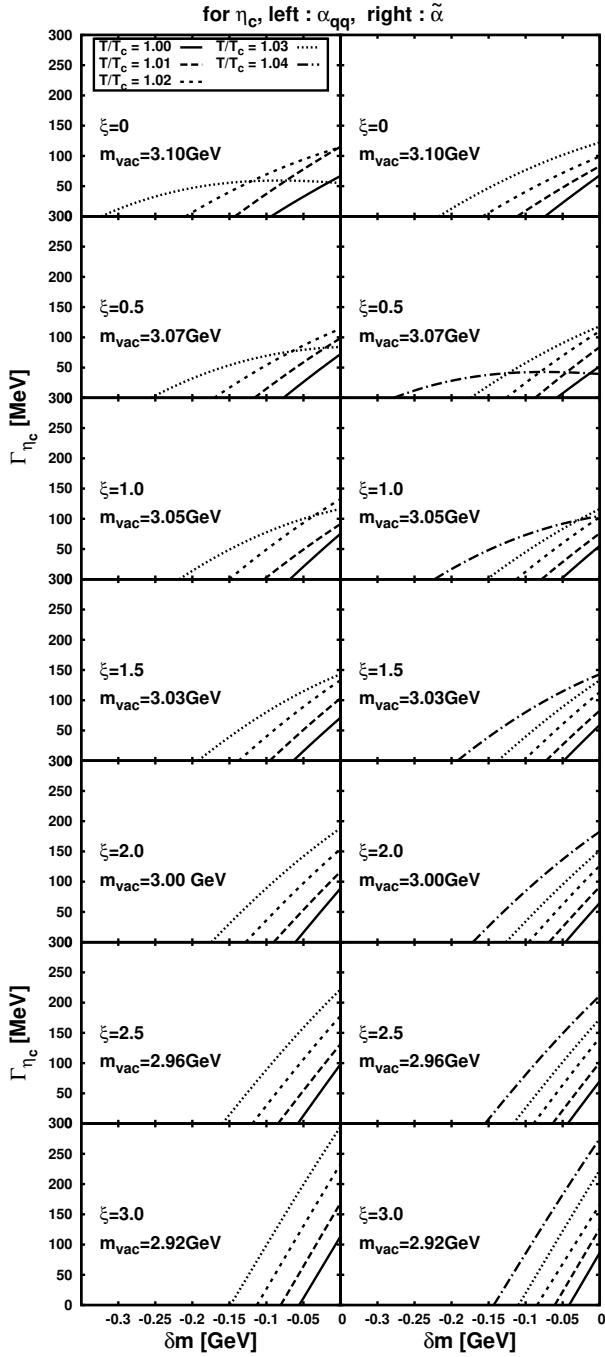


FIG. 11: Same as Fig. 10, but for η_c .

curves become almost parallel among large ξ results, as a consequence of the better stability. From the nature of the phenomenological side shown in Fig. 4, this case corresponds to the maximum mass shift. The mass shift shows ~ 50 MeV reduction from vacuum to T_c , and it increases additionally by ~ 20 -50 MeV as temperature rises by $0.01T_c$. Consequently, it becomes 100-300 MeV at $T = 1.04T_c$.

Similarly, Fig. 13 shows that the width begins to increase with temperature across T_c if no mass shift takes

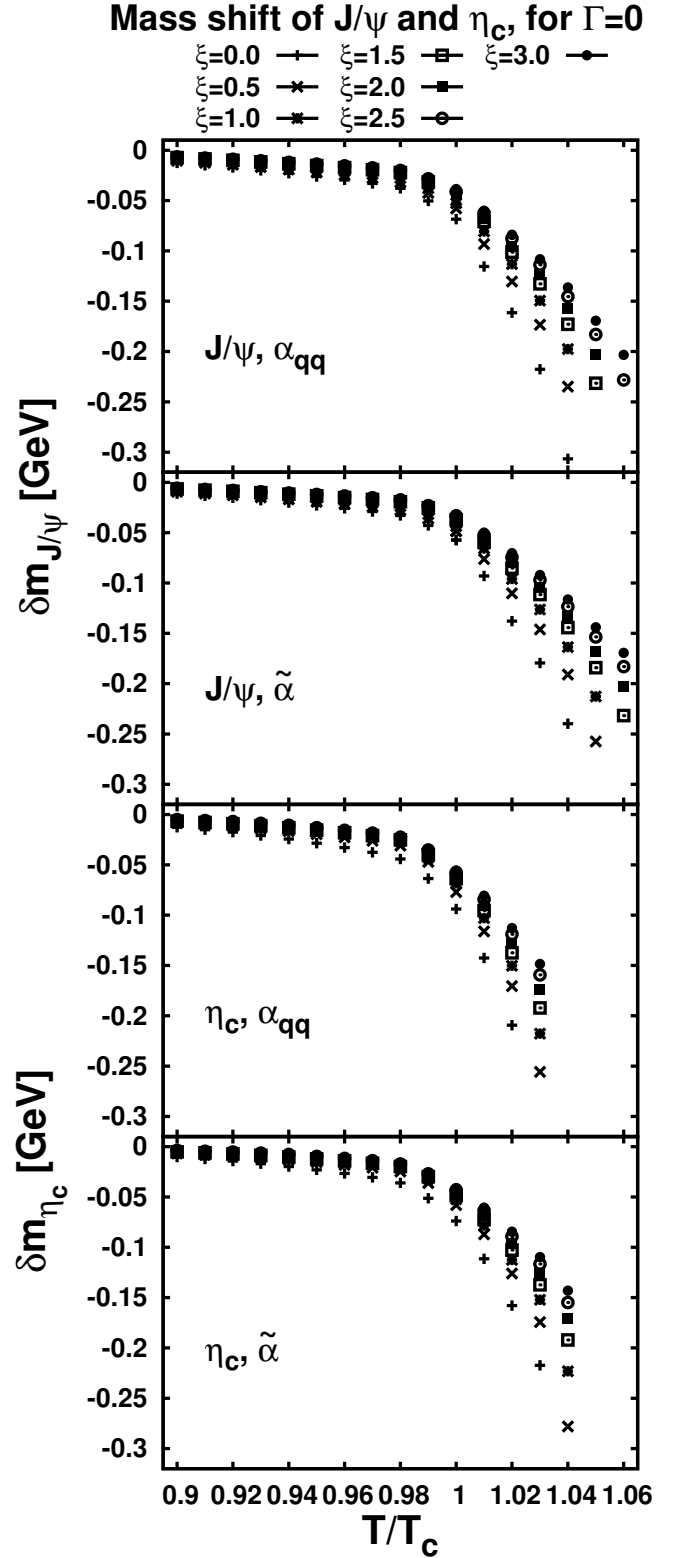


FIG. 12: Temperature dependence of the masses in the $\Gamma \rightarrow 0$ limit. Symbols stand for different ξ values.

place. This also shows almost linear dependence on tem-

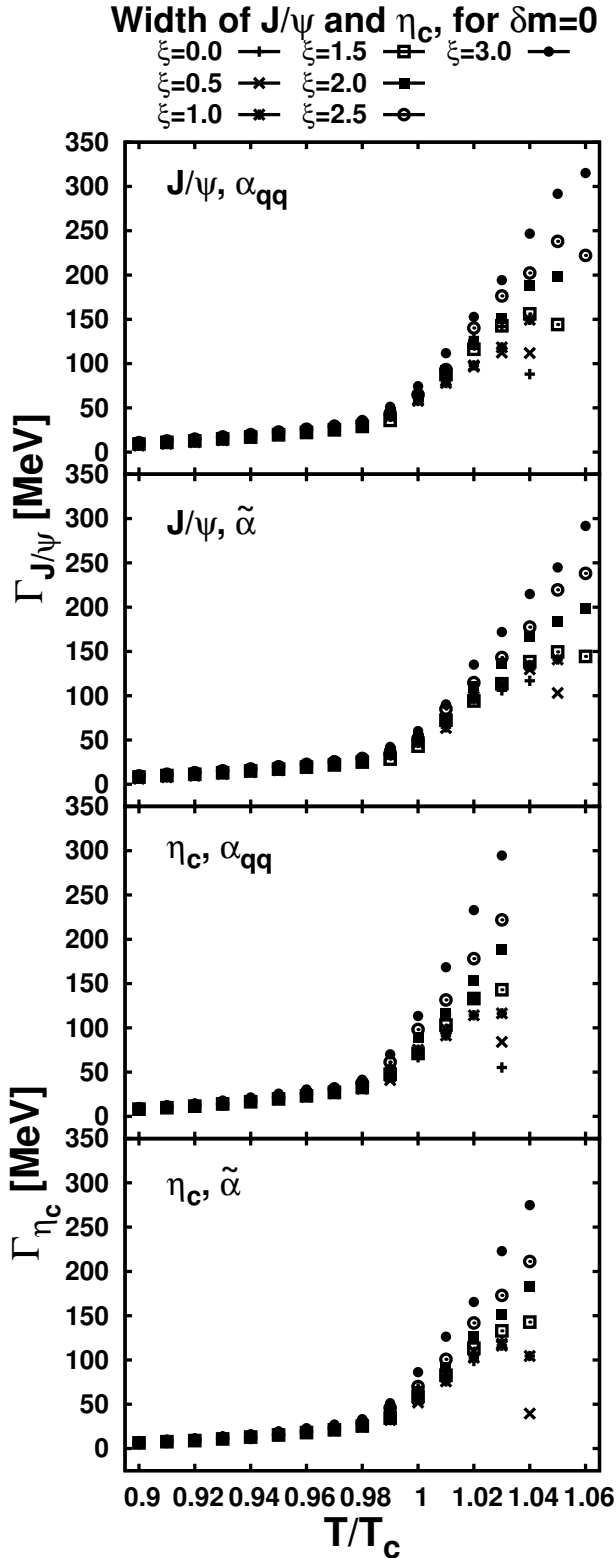


FIG. 13: Temperature dependence of the widths in the $m \rightarrow 0$ limit. Symbols are the same as in Fig. 12.

perature above T_c . Though some exceptions can be seen

in the small ξ results, which are also indicated in Figs. 10 and 11, these behaviors come from the vague stability appearing as too large n in Table I. Hence, we can conclude that the width increases linearly with temperature above T_c if the mass remains unchanged. Since we did not do fine tuning of the parameters for each ξ , the values of mass shift and width differ for different ξ . However, the qualitative features do not depend on ξ where the stability is reliable. This shows robustness of our analysis. A realistic change at each temperature should be a combined decrease in mass and increase in width, whose values are smaller than their maximal changes obtained here. However, to determine the realistic combination, we need to have an additional constraint between the changes in the width and the mass, or input the thermal width from another calculation.

IV. NUCLEAR MATTER

In this section, we analyze change of mass and width of the charmonium induced by nuclear medium with the same framework that was implemented in the previous section. Here, we use Eqs. (25) and (26) instead of Eqs. (13) and (14), respectively. With the common parameter set, the condensates are $\phi_b = 1.74 \times 10^{-3}$ for vacuum, 1.64×10^{-3} for the nuclear matter, and $\phi_c = -1.28 \times 10^{-5}$.

As previously shown in Ref. [21], the change of mass, which is identical to the change of the moment ratio of the OPE side [Eq.(29)], is not as large as in the hot gluonic matter case. Thus we do not have to worry about the stability of the OPE. Nevertheless, increasing ξ improves the validity of the OPE. We will show the results for $0 \leq \xi \leq 3$ as well as in the hot gluonic matter case to show the robustness and the consistency of the calculation.

TABLE II: List of n which stabilize the moment ratio for the nuclear matter

| channel | $\xi = 0$ | $\xi = 0.5$ | $\xi = 1$ | $\xi = 1.5$ | $\xi = 2$ | $\xi = 2.5$ | $\xi = 3$ |
|----------|-----------|-------------|-----------|-------------|-----------|-------------|-----------|
| J/ψ | 5 | 7 | 9 | 10 | 12 | 13 | 14 |
| η_c | 6 | 8 | 10 | 12 | 14 | 15 | 17 |

We list values of n in which the moment ratio of the OPE side for nuclear medium becomes minimum in Table II. The vacuum case has been already shown in Table I. Comparing these two cases, we can see that the values of n are the same except for a few exception in the J/ψ case, by virtue of the small shift of the gluon condensates in the nuclear matter. In such exceptional cases, difference of the values of the moment ratio from the same n value case with the vacuum is almost negligible. *i.e.*, the moment ratio is almost constant around these n .

We plot the width Γ as a function of the mass shift δm in Fig. 14 as well as in the GP case. In both J/ψ and η_c

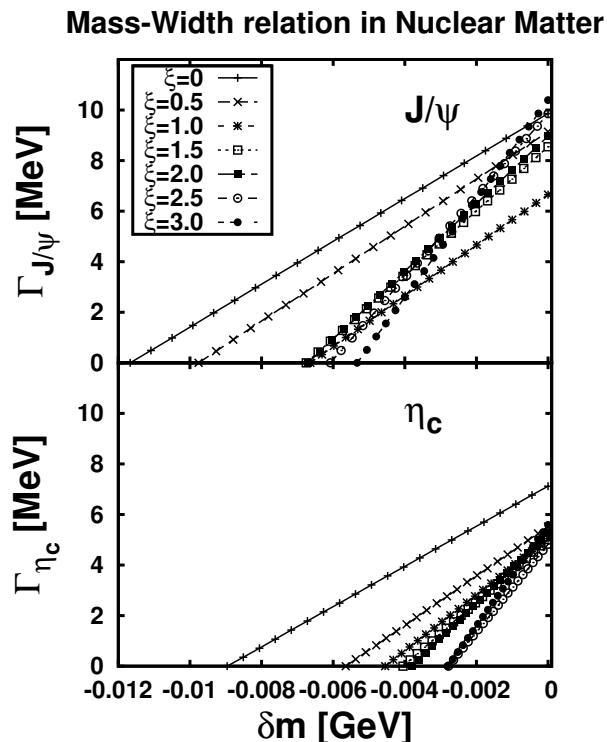


FIG. 14: Relation between mass shift and width in the nuclear matter.

cases, smaller ξ than 1.5 show larger mass shift and width broadening but larger ξ results agree each other. From the stability argument, larger ξ results will be more reliable. Then, possible mass shifts are maximally -7 MeV for J/ψ and -4 MeV η_c while maximum widths are 10 MeV for J/ψ and 6 MeV for η_c .

V. DISCUSSION AND SUMMARY

In Sec. III, we have shown that mass decreases suddenly across T_c and the shift reaches maximally a few hundred MeV above T_c in the hot gluonic matter. Alternatively, width can also maximally broaden to ~ 200 MeV. Although our analysis cannot determine both of mass and width simultaneously, this is a notable result which should be examined in the present and future experiments. In fact, a next to leading order QCD calculation shows that the thermal width of J/ψ slight above T_c is smaller than a few 10 MeV [40, 41]. Hence a large mass shift will take place. Note that such a large mass shift has been expected from different points view; AdS/QCD [42] and the sudden reduction of the asymptotic value of the potential seen in lattice QCD [43] which leads to lowering of the bound state energy [44]. Recent lattice QCD calculation based on the maximum entropy method also shows non-trivial shift of the peak in the spectral function above T_c [45]. Since our results access only near T_c , we are still far from the complete understanding of the be-

havior of the charmonium in the deconfined medium. In the most plausible picture from the current understanding, charmonia are melting at very high temperature expected in the early stage of the heavy ion collisions at RHIC and LHC. Then the pairs of heavy quark and antiquark form the bound states at a certain temperature which depends on quantum number. The temperature is expected as $\sim 2T_c$ for J/ψ at RHIC [46]. After charmonia are produced, they will dissociate by collisions with partons. If this phase lasts long enough compared to the inverse of the width, the charmonia can decay in the medium. In fact, the lifetime of the partonic medium is about 4-5 fm/c in a hydrodynamic calculation for the central Au+Au collisions at the maximum RHIC energy [47]. This will be much longer at LHC. From Fig. 10, we expect ~ 200 MeV J/ψ mass reduction in the case of the small decay width. This shift is larger than experimental mass resolutions (~ 35 MeV for dielectron channel of PHENIX at RHIC [8], 33 MeV for dielectron channel and 75 MeV for dimuon channel of ALICE at LHC [48]).

Alternatively, statistical hadronization near phase boundary has been also examined [49]. In this case, the number of produced charmonium will be enhanced if the notable mass shift occurs. For example, there may be a factor of 2 enhancement for $T = 170$ MeV and $\delta m = -100$ MeV since the enhancement factor is given by $e^{-\delta m/T}$. This enhancement might be observed by comparing particle ratio.

As for the nuclear medium result, we have extended the analysis carried out in Ref. [21] to the one which takes account of finite width. We have also shown the results for different ξ values. Since we have given the relation between the mass shift and width, we can estimate the mass shift in the presence of finite width effect by considering the dissociation cross section of the charmonium by nucleon. Provided the Fermi momentum is $p_F \simeq 250$ MeV and the cross section is $\sigma_{J/\psi-N} \simeq 2\text{mb}$, the decay width $\Gamma = \langle \sigma_{J/\psi-N} v_{\text{rel}} \rho_N \rangle$ becomes ~ 1.3 MeV for charmonium at rest. The cross section may be smaller, because the incident momentum is considered to be small and the process will be near threshold. From this estimate, if we take into account the broadening of the width, the mass shift becomes slightly smaller, by about 0.5 MeV, according to the results shown in Fig. 14. Therefore, this justifies the argument in Ref. [21] that the influence of the decay widths is expected to be small.

The change of spectral properties in the nuclear matter can be experimentally investigated by Panda experiment at GSI-FAIR in which incident anti-proton collide with nuclear target. Here we present some predictions for cross sections of charmonium production through $\bar{p}p$ annihilation and subsequent decay into dileptons or radiative decay in the experiment. We compute the cross sections with the Breit-Wigner formula

$$\sigma_{\text{BW}}(s) = \frac{B_{\text{in}} B_{\text{out}} (2J+1)}{(2s_1+1)(2s_2+1) k_{\text{cm}}^2} \frac{4\pi}{(s-m^2)^2 + s\Gamma_{\text{tot+med}}^2} \frac{s\Gamma_{\text{tot}}^2}{(31)}$$

TABLE III: Parameters and results in charmonium productions at GSI-FAIR. Cross sections and event per day correspond to the case of maximum medium width, $\Gamma_{\text{med}} = 20$ MeV.

| Resonance | m [MeV] | δm [MeV] | Γ_{tot} | Final State | $\overline{\sigma}_{\text{BW}}$ at peak | Events per day |
|-------------|-----------|------------------|-----------------------|-------------------|---|----------------|
| J/ψ | 3097 | -7 | 93.4keV | $e^+ + e^-$ | 0.435 pb | 7.5 |
| η_c | 2980 | -4 | 25.5MeV | $e^+ + e^-$ | 10.7 pb | 184 |
| χ_{c0} | 3415 | -60 | 10.4MeV | $J/\psi + \gamma$ | 18.0 pb | 311 |
| χ_{c1} | 3511 | -60 | 0.89MeV | $J/\psi + \gamma$ | 4.5 pb | 78 |
| χ_{c2} | 3556 | -60 | 2.05MeV | $J/\psi + \gamma$ | 19.8 pb | 343 |

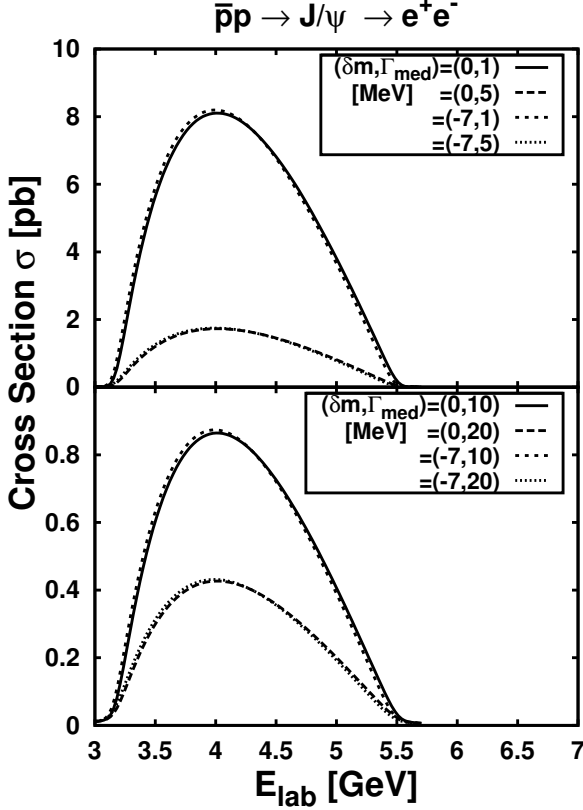


FIG. 15: Cross section of J/ψ production in $\bar{p} - A$ collisions. Upper panel shows smaller medium width (1 and 5 MeV) cases and lower one shows larger (10 and 20 MeV) cases for with and without mass shift.

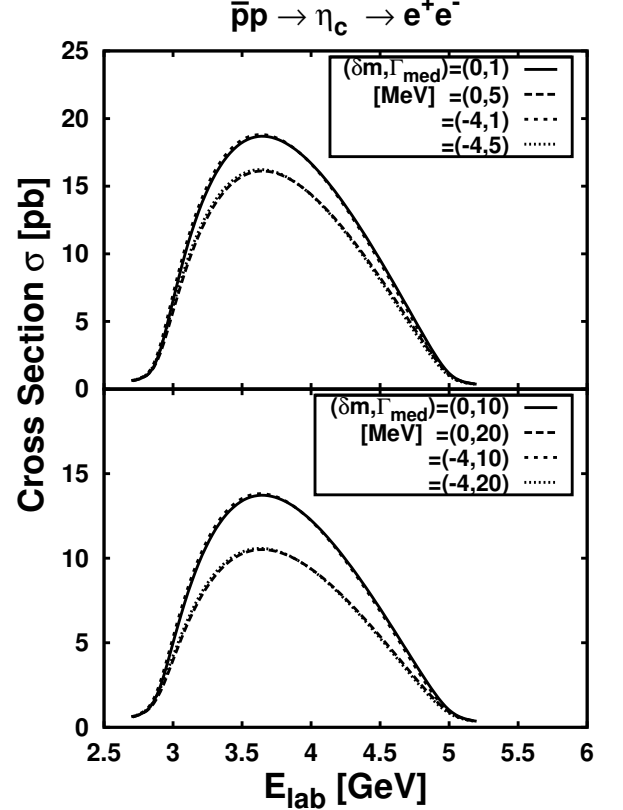


FIG. 16: Same as Fig. 15, but for η_c .

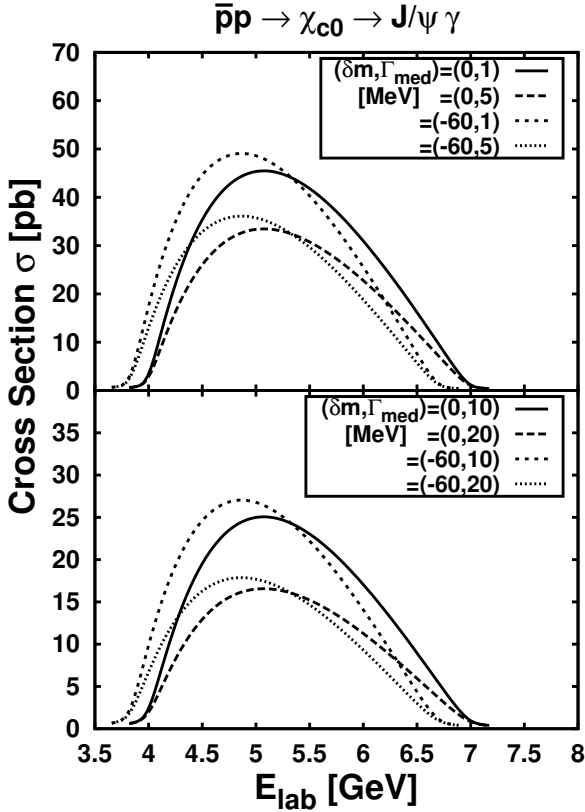
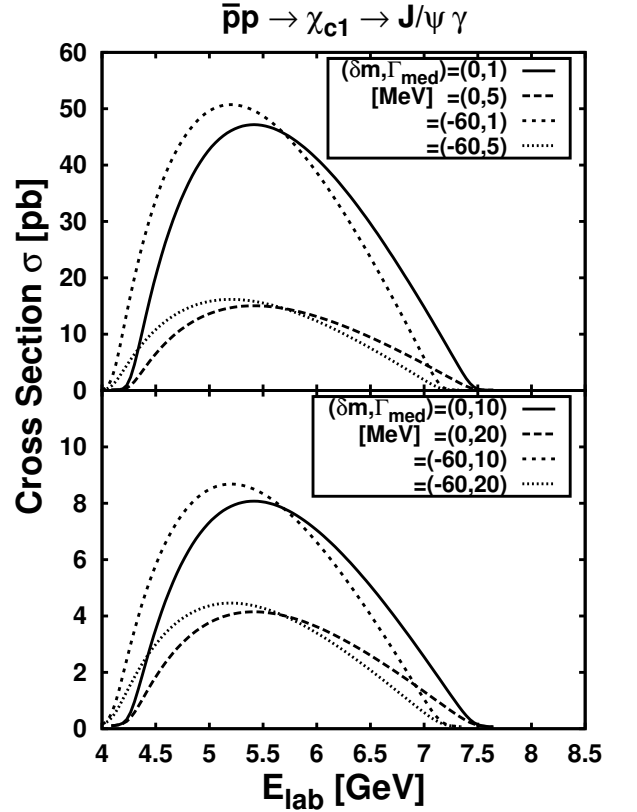
where s , k_{cm}^2 and m are the Mandelstam variable, c.m. momentum and mass of charmonium with spin J , respectively. Γ_{tot} is the total decay width of the charmonium and $\Gamma_{\text{tot}+\text{med}} = \Gamma_{\text{tot}} + \Gamma_{\text{medium}}$. B_{in} and B_{out} are the branching fraction of the resonance into the entrance and exit channels. s_i is the spin of the incident particles, which are anti-protons and protons in the present calculation. Since the target protons are in nucleus, we have to take the Fermi motion into account for accurate estimation. We average the Breit-Wigner cross section

with respect to target momentum as

$$\overline{\sigma}_{\text{BW}} = \frac{4}{\rho_0} \int_0^{k_F} k^2 \frac{dk d\Omega}{(2\pi)^3} \sigma_{\text{BW}}. \quad (32)$$

In addition to J/ψ and η_c , we also calculate cross sections for χ_c which are expected to show larger mass shift $\delta m \simeq -40 \sim -60$ MeV [50]. Parameters in the calculations are summarized in Table III. Γ_{medium} is treated as a free parameter varied from 1 MeV to 20 MeV.

Results of the cross sections as a function of incident anti-proton energy are shown in Fig. 15-19. We can clearly see that sharp peaks of the resonances disappear. This is because of the Fermi motion of the target protons in the nucleus. For example, incident energy to create J/ψ (3097) is $E_{\text{lab}} = 4.17$ GeV, but the fluctua-

FIG. 17: Same as Fig. 15, but for χ_{c0} .FIG. 18: Same as Fig. 15, but for χ_{c1} .

tion of the target momentum makes it possible to create J/ψ with $3.17 \leq E_{\text{lab}} \leq 5.51$ GeV, in which the minimum and the maximum E_{lab} correspond to the target momentum along the collision axis $p_{2z} = -k_F$ and k_F , respectively. This effect considerably broadens the cross section. Consequently, one needs no fine tuning of incident proton energy to produce charmonium. For J/ψ and η_c , mass shifts are so small that the peak positions of incident energy do not change. However, mass shift of χ_c , ~ -60 MeV, is sufficiently large to show clear shift of the peak in the cross section. In these calculations, we treat Γ_{medium} as a free parameter. It is shown that this parameter affects only on the magnitude of the cross section, which is larger for smaller change from the vacuum width. Hence, though we cannot predict both of mass shift and in-medium width, we can obtain information on both quantities from the experimentally measured cross sections. We summarized the cross sections and expected event rate at GSI-FAIR, of which luminosity is expected to be $2 \times 10^{32} \text{cm}^{-2} \text{s}^{-1}$, in last two column of Table. III. We can see that the expected event rates are large enough for the mass shift of χ_c to be observed.

Finally we address possible improvements of this work. Since we restricted ourselves to the hot medium which consists of gluons only in the first part of this paper, we should take the quarks into account for more realistic estimation. It is an easy task to use the gluon condensates

data obtained from full lattice calculation. However, we will have to take into account the scattering and continuum terms due to thermal charm quarks. Physically effects of these terms will not be so large; a full lattice QCD calculation based on MEM shows also similar mass shift of charmonium [45]. Furthermore, a recent study on D meson at finite temperature suggests they dissolves above T_c [51]. This means charm quarks in the deconfined phase do not have light meson modes and thus will be free. Although there might be non-trivial thermal mass, the scattering term will cancel out between the OPE side and the phenomenological side in the deconfined medium.

It is also important to study change of χ_c at finite temperature, which may influence the quantitative feature of the sequential melting [52], since non-negligible fraction of J/ψ comes from decay of ψ' and χ_c in relativistic heavy ion collisions. This can be done by calculating Wilson coefficients for tensor operators for these channels. It should be also noted that the continuum part of the spectral function may play an important role. This will be possible by modeling the medium with a gas of quasi-particle. One more thing to be done is the extension to higher temperature. The failure of $T > 1.06T_c$ for J/ψ and $T > 1.04T_c$ for η_c originates from the instability of the moment ratio of the OPE side. The twist-2 gluon condensates becomes larger as temperature increases and

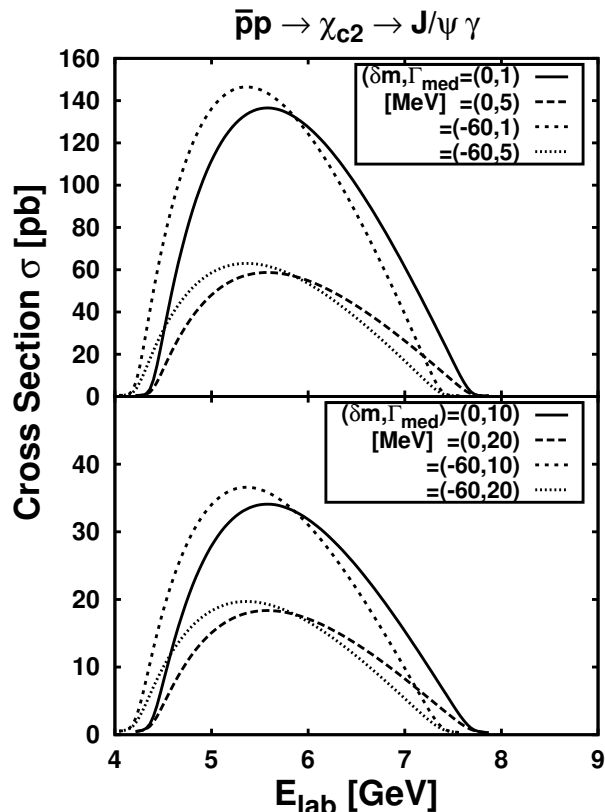


FIG. 19: Same as Fig. 15, but for χ_{c2} .

then leads to the breakdown of the stability in the OPE side including up to dimension 4 (see Fig. 9) and $\mathcal{O}(\alpha_s)$. In Fig. 7, we can also see that the expansion is not good at large n that stabilize the moment ratio at higher temperature. These facts suggest the necessity of including higher dimensional operators, which is examined in Ref. [53]. However, we do not know a simple way to extract the temperature dependencies of the higher dimensional operators from the lattice calculation, as was done in the present work for dimension 4 operators. The other way of the extension is to improve the phenomenological side such that it includes temperature dependent continuum contribution. The decrease of the scalar gluon condensates above T_c indicates perturbative contribution becomes more important at higher temperature. If we can construct a more appropriate phenomenological side reflecting the nature of the strongly interacting matter, it will lead to n -independent results for physical parameters

until the charmonia really dissolve.

We also note that there are some spaces to improve the analyses for nuclear matter. Especially, the present analysis shows the mass shift of χ_c states are likely to be observed in the forthcoming experiment. However, the current estimate of the mass shift is not a decisive one; we have to take the twist-2 contribution into account for a more accurate estimation.

In summary, we have given a comprehensive analysis on medium-induced change of the spectral properties of J/ψ and η_c in the hot gluonic medium and the nuclear medium by making use of QCD sum rules. In the case of the gluonic medium, our analysis shows there must be a notable change of mass or width, or both around T_c , caused by the rapid change of the gluon condensates. Although the present formalism is found to be applicable only up to $T \simeq 1.06T_c$, the change of mass and width can maximally reach a few hundred MeV. We have discussed its implication for future heavy ion experiment at CERN-LHC. As for the nuclear matter case, we extend the past works to include small but finite width and check the robustness by varying the scale parameter of the theory. We also examined the possibility of detecting such mass shifts in the future experiment at GSI-FAIR. Although J/ψ and η_c do not show prominent signals, χ_c exhibits more promising results. These analyses give the basis of future improvements to study the nature of the strongly interacting matter deeply with charmonia.

Acknowledgments

This work was supported by BK21 Program of the Korean Ministry of Education. S. H. L. was supported by the Korean Research Foundation KRF-2006-C00011 and by the Yonsei University research fund. K. M. would like to thank the members of the high energy physics group of Waseda University for allowing him to use their workstations. He also would like to acknowledge T. Hatsuda for his fruitful comments and discussions.

APPENDIX A: WILSON COEFFICIENTS

Here we list explicit forms of the Wilson coefficients which appear in Eq. (10) and are originally given in Refs. [19] and [21]. In the following, $\rho = \xi/(1 + \xi)$ and $F(a, b, c; x)$ is the hypergeometric function ${}_2F_1(a, b, c; x)$.

For the pseudoscalar channel,

$$A_n^P(\xi) = \frac{3}{8\pi^2} \frac{2^n(n-1)!}{(2n+1)!!} (4m^2)^{-n} (1+\xi)^{-n} F(n, 1/2, n+3/2; \rho) \quad (\text{A1})$$

$$a_n^P(\xi) = \frac{(2n+1)!!}{3 \cdot 2^{n-1}n!} \left[\pi - \frac{1}{2(n+1)} \left(\frac{1}{2}\pi - \frac{3}{4\pi} \right) F(n, 1, n+2; \rho) \right] \frac{1}{F(n, 1/2, n+3/2; \rho)} - \left(\frac{1}{2}\pi - \frac{3}{4\pi} \right) + \frac{1}{\pi} \left[\frac{8}{3} - \frac{4}{n} \frac{F(n, 3/2, n+3/2; \rho)}{F(n, 1/2, n+3/2; \rho)} - \frac{5}{6} \frac{1}{n+3/2} \frac{F(n, 3/2, n+5/2; \rho)}{F(n, 1/2, n+3/2; \rho)} \right] - 2n \frac{\ln(2+\xi)}{\pi} \frac{(2+\xi)}{(1+\xi)^2} \frac{F(n+1, 1/2, n+3/2; \rho)}{F(n, 1/2, n+3/2; \rho)}, \quad (\text{A2})$$

$$b_n^P(\xi) = -\frac{n(n+1)(n+2)(n+3)}{2n+3} (1+\xi)^{-1} \left[\frac{F(n+1, -3/2, n+5/2; \rho)}{F(n, 1/2, n+3/2; \rho)} - \frac{6}{n+3} \frac{F(n+1, -1/2, n+5/2; \rho)}{F(n, 1/2, n+3/2; \rho)} \right], \quad (\text{A3})$$

$$c_n^P(\xi) = b_n^P(\xi) - \frac{4n(n+1)}{(1+\xi)} \frac{F(n+1, -1/2, n+3/2; \rho)}{F(n, 1/2, n+3/2; \rho)}. \quad (\text{A4})$$

Similarly, for the vector channel,

$$A_n^V(\xi) = \frac{3}{4\pi^2} \frac{2^n(n+1)(n-1)!}{(2n+3)!!} \frac{F(n, 1/2, n+5/2; \rho)}{[(4m^2)(1+\xi)]^n}, \quad (\text{A5})$$

$$a_n^V(\xi) = \frac{(2n+1)!!}{3 \cdot 2^{n-1}n! F(n, 1/2, n+5/2; \rho)} \left(\frac{2n+3}{2n+2} \right) \left[\pi - \left\{ \frac{\pi}{3} + \frac{1}{2} \left(\frac{\pi}{2} - \frac{3}{4\pi} \right) \right\} \frac{F(n, 1, n+2; \rho)}{n+1} + \frac{F(n, 2, n+3; \rho)}{3(n+1)(n+2)} \left(\frac{\pi}{2} - \frac{3}{4\pi} \right) \right] - \left(\frac{\pi}{2} - \frac{3}{4\pi} \right) - 2n \frac{\ln(2+\xi)}{\pi} \frac{(2+\xi)}{(1+\xi)^2} \frac{F(n+1, 1/2, n+7/2; \rho)}{F(n, 1/2, n+5/2; \rho)}, \quad (\text{A6})$$

$$b_n^V(\xi) = -\frac{n(n+1)(n+2)(n+3)}{(2n+5)(1+\xi)^2} \frac{F(n+2, -1/2, n+7/2; \rho)}{F(n, 1/2, n+5/2; \rho)}, \quad (\text{A7})$$

$$c_n^V(\xi) = b_n^V(\xi) - \frac{4n(n+1)}{3(2n+5)(1+\xi)^2} \frac{F(n+2, 3/2, n+7/2; \rho)}{F(n, 1/2, n+5/2; \rho)}. \quad (\text{A8})$$

In Eqs. (A1) and (A5), m is the running quark mass $m = m_c(p^2 = -(\xi+1)m_c^2)$ which is given by [54],

$$\frac{m_c(\xi)}{m_c(\xi=0)} = 1 - \frac{\alpha_s}{\pi} \left[\frac{2+\xi}{1+\xi} \ln(2+\xi) - 2 \ln 2 \right] \quad (\text{A9})$$

-
- | | |
|--|---|
| <p>[1] I. Arsene et al. (BRAHMS Collaboration), Nucl. Phys. A757, 1 (2005).</p> <p>[2] B. B. Back et al. (PHOBOS Collaboration), Nucl. Phys. A757, 28 (2005).</p> <p>[3] J. Adams et al. (STAR Collaboration), Nucl. Phys. A757, 102 (2005).</p> <p>[4] K. Adcox et al. (PHENIX Collaboration), Nucl. Phys. A757, 184 (2005).</p> <p>[5] M. Gyulassy and L. McLerran, Nucl. Phys. A750, 30 (2005).</p> <p>[6] T. Matsui and H. Satz, Phys. Lett. B 178, 416 (1986).</p> <p>[7] S. S. Adler et al. (PHENIX Collaboration), Phys. Rev. C 69, 014901 (2004).</p> <p>[8] A. Adare et al. (PHENIX Collaboration), Phys. Rev. Lett. 98, 232301 (2007).</p> <p>[9] D. E. Kharzeev, J. Phys. G: Nucl. Part. Phys. 34, S445 (2007).</p> <p>[10] A. Andronic, P. Braun-Munzinger, K. Redlich, and</p> | <p>J. Stachel, Phys. Lett. B 652, 259 (2007).</p> <p>[11] T. Umeda, R. Katayama, O. Miyamura, and H. Matsu-furu, Int. J. Mod. Phys. A 16, 2215 (2001).</p> <p>[12] M. Asakawa and T. Hatsuda, Phys. Rev. Lett. 92, 012001 (2004).</p> <p>[13] S. Datta, F. Karsch, P. Petreczky, and I. Wetzorke, Phys. Rev. D 69, 094507 (2004).</p> <p>[14] T. H. Hansson, S. H. Lee, and I. Zahed, Phys. Rev. D 37, 2672 (1988).</p> <p>[15] S. J. Brodsky, I. Schmidt, and G. F. de Téramond, Phys. Rev. Lett. 64, 1011 (1990).</p> <p>[16] M. A. Shifman, A. I. Vainshtein, and V. I. Zakharov, Nucl. Phys. B147, 385 (1979).</p> <p>[17] M. A. Shifman, A. I. Vainshtein, and V. I. Zakharov, Nucl. Phys. B147, 448 (1979).</p> <p>[18] J. P. Blaizot, J. Phys. G: Nucl. Part. Phys. 34, S243 (2007).</p> <p>[19] L. J. Reinders, H. R. Rubinstein, and S. Yazaki, Nucl.</p> |
|--|---|

- Phys. **B186**, 109 (1981).
- [20] R. J. Furnstahl, T. Hatsuda, and S. H. Lee, Phys. Rev. D **42**, 1744 (1990).
- [21] F. Klingl, S. Kim, S. H. Lee, P. Morath, and W. Weise, Phys. Rev. Lett. **82**, 3396 (1999).
- [22] A. Hayashigaki, Prog. Theor. Phys. **101**, 923 (1999).
- [23] K. Morita and S. H. Lee, to be published in Phys. Rev. Lett., arXiv:0704.2021 [nucl-th].
- [24] K. G. Wilson, Phys. Rev. **179**, 1499 (1969).
- [25] S. C. Generalis and D. J. Broadhurst, Phys. Lett. **139B**, 85 (1984).
- [26] E. M. Lifshitz and L. P. Pitaevskii, *Statistical Physics, Part 2*, vol. 9 of *Course of Theoretical Physics* (Butterworth-Heinemann, 1980).
- [27] T. Hatsuda, Y. Koike, and S. H. Lee, Nucl. Phys. **B394**, 221 (1993).
- [28] A. I. Bochkarev and M. E. Shaposhnikov, Nucl. Phys. **B268**, 220 (1986).
- [29] O. Kaczmarek, F. Karsch, F. Zantow, and P. Petreczky, Phys. Rev. D **70**, 074505 (2004).
- [30] A. D. Giacomo and G. C. Rossi, Phys. Lett. B **100**, 481 (1981).
- [31] A. D. Giacomo and G. Paffuti, Phys. Lett. B **108**, 327 (1982).
- [32] M. Campostrini and A. D. Giacomo, Phys. Lett. B **197**, 403 (1987).
- [33] S. H. Lee, Phys. Rev. D **40**, 2484 (1989).
- [34] D. E. Miller, Phys. Rept. **443**, 55 (2007).
- [35] G. Boyd, J. Engles, F. Karsch, E. Laermann, C. Legeland, M. Lütgemeier, and B. Petersson, Nucl. Phys. **B469**, 419 (1996).
- [36] T. D. Cohen, R. J. Furnstahl, and D. K. Griegel, Phys. Rev. C **45**, 1881 (1992).
- [37] B. Borasoy and U. G. Meißner, Phys. Lett. B **365**, 285 (1996).
- [38] S. Leupold, W. Peters, and U. Mosel, Nucl. Phys. **A628**, 311 (1998).
- [39] W. H. Press, S. A. Teukolsky, W. T. Vetterling, and B. P. Flannery, *Numerical Recipes in Fortran 90* (Cambridge University Press, 1996), chap. 7.
- [40] Y. Park, K. I. Kim, T. Song, S. H. Lee, and C. Y. Wong, Phys. Rev. C **76**, 044907 (2007).
- [41] S. H. Lee, Y. Park, K. I. Kim, and T. Song, J. Phys. G: Nucl. Part. Phys. **34**, S843 (2007).
- [42] Y. Kim, J. P. Lee, and S. H. Lee, Phys. Rev. D **75**, 114008 (2007).
- [43] F. Karsch and E. Laermann, in *Quark-Gluon Plasma 3*, edited by R. C. Hwa and X. N. Wang (World Scientific, 2004), p. 1, hep-lat/0305025.
- [44] C. Y. Wong, Phys. Rev. C **72**, 034906 (2005).
- [45] G. Aarts, C. Allton, M. B. Oktay, M. Peardon, and J.-I. Skullerud, arXiv:0705.2198[hep-lat].
- [46] T. Gunji, H. Hamagaki, T. Hatsuda, and T. Hirano, Phys. Rev. C **76**, 051901(R) (2007).
- [47] K. Morita, Braz. J. Phys. **37**, 705 (2007).
- [48] B. Alessandro et al. (ALICE Collaboration), J. Phys. G: Nucl. Part. Phys. **32**, 1295 (2006).
- [49] A. Andronic, P. Braun-Munzinger, K. Redlich, and J. Stachel, Nucl. Phys. **A789**, 334 (2007).
- [50] S. H. Lee, AIP Conf. Proc. **717**, 780 (2004).
- [51] C. A. Dominguez, M. Loewe, and J. C. Rojas, arXiv:0707.2844[hep-ph].
- [52] F. Karsch, D. Kharzeev, and H. Satz, Phys. Lett. B **637**, 75 (2006).
- [53] S. Kim and S. H. Lee, Nucl. Phys. **A679**, 517 (2001).
- [54] V. A. Novikov, L. B. Okun, M. A. Shifman, A. I. Vainshtein, M. B. Voloshin, and Z. I. Zakharov, Phys. Rept **41**, 1 (1978).